




Detection of elemental magnetization reversal events in a micro-patterned Nd-Fe-B hot-deformed magnet

Cite as: AIP Advances **9**, 125052 (2020); <https://doi.org/10.1063/1.5129830@adv.2020.MMM2020.issue-1>

Submitted: 03 October 2019 . Accepted: 21 November 2019 . Published Online: 30 December 2019

Takahiro Yomogita, Nobuaki Kikuchi , Satoshi Okamoto, Osamu Kitakami, Hossein Sepehri-Amin , Tadakatsu Ohkubo, Kazuhiro Hono , Keiko Hioki, and Atsushi Hattori

COLLECTIONS

Paper published as part of the special topic on [64th Annual Conference on Magnetism and Magnetic Materials](#) and [Collection](#)

Note: This paper was presented at the 64th Annual Conference on Magnetism and Magnetic Materials.



View Online



Export Citation



CrossMark

ARTICLES YOU MAY BE INTERESTED IN

[Coercivity enhancement of Nd-Fe-B hot-deformed magnets by the eutectic grain boundary diffusion process using Nd-Ga-Cu and Nd-Fe-Ga-Cu alloys](#)

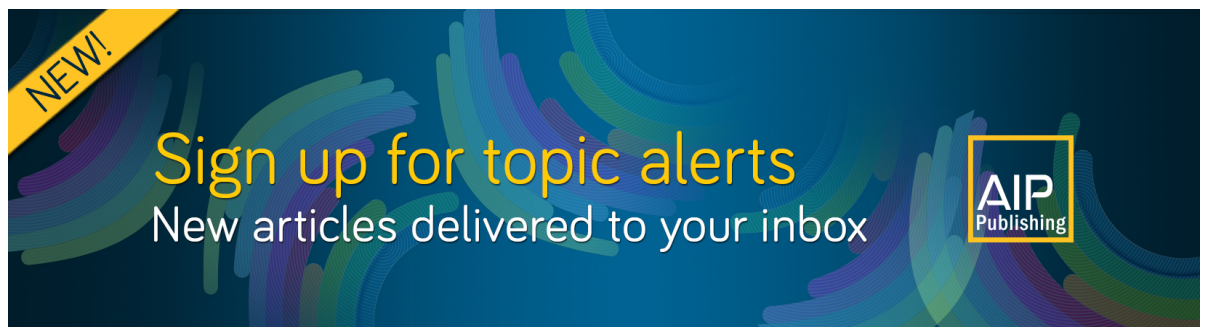
AIP Advances **8**, 056205 (2018); <https://doi.org/10.1063/1.5006575>

[Observation of anomalous Ettingshausen effect and large transverse thermoelectric conductivity in permanent magnets](#)

Applied Physics Letters **115**, 222403 (2019); <https://doi.org/10.1063/1.5131001>


[Direct observation of ferromagnetism in grain boundary phase of Nd-Fe-B sintered magnet using soft x-ray magnetic circular dichroism](#)

Applied Physics Letters **105**, 202404 (2014); <https://doi.org/10.1063/1.4902329>



NEW!

Sign up for topic alerts
New articles delivered to your inbox






Detection of elemental magnetization reversal events in a micro-patterned Nd-Fe-B hot-deformed magnet

Cite as: AIP Advances 9, 125052 (2019); doi: 10.1063/1.5129830

Presented: 6 November 2019 • Submitted: 3 October 2019 •

Accepted: 21 November 2019 • Published Online: 30 December 2019



Takahiro Yomogita,^{1,a)} Nobuaki Kikuchi,¹  Satoshi Okamoto,^{1,2,a)} Osamu Kitakami,¹ Hossein Sepeshri-Amin,² 
Tadakatsu Ohkubo,² Kazuhiro Hono,²  Keiko Hioki,³ and Atsushi Hattori⁴

AFFILIATIONS

¹Institute of Multidisciplinary Research for Advanced Materials, Tohoku University, Sendai 980-8577, Japan

²Elements Strategy Initiative Center for Magnetic Materials, National Institute for Materials Science, Tsukuba 305-0047, Japan

³Daido Steel Co., Ltd., Nagoya 461-8581, Japan

⁴Daido Electronical Co., Ltd., Nakatsugawa 509-9132, Japan

Note: This paper was presented at the 64th Annual Conference on Magnetism and Magnetic Materials.

^{a)}Electronic addresses: takahiro.yomogita.s4@dc.tohoku.ac.jp and satoshi.okamoto.c1@tohoku.ac.jp

ABSTRACT

Magnetization reversal in a permanent magnet takes place through multiple and simultaneous events of nucleation and domain wall depinning. Thus, detection and analysis of elemental magnetization reversal events are essentially important to understand the coercivity mechanism of a permanent magnet. In this study, we have fabricated a micro-patterned Nd-Fe-B hot-deformed magnet using mechanical polishing and focused ion beam, and anomalous Hall effect (AHE) detection has been adopted to measure the magnetization reversal of the sample. During the micro-patterning process, the degradation of magnetic property is carefully evaluated. Consequently, the micro-patterned Nd-Fe-B hot-deformed magnet with the thick of 5 μm and the width of 13 μm is fabricated, and subsequently, the discrete steps on the AHE curve are successfully detected. The magnetization reversal unit size estimated from the step height is $\sim 1 \mu\text{m}^2$, which is almost the same as observed in the magneto-optical Kerr microscopy. We have clearly demonstrated that this technique has significant potential to study the physical nature of elemental magnetization reversal events in permanent magnets.

© 2019 Author(s). All article content, except where otherwise noted, is licensed under a Creative Commons Attribution (CC BY) license (<http://creativecommons.org/licenses/by/4.0/>). <https://doi.org/10.1063/1.5129830>

I. INTRODUCTION

Since Nd-Fe-B magnets exhibit the highest maximum energy product $(BH)_{\text{max}}$ among all of permanent magnetic materials,^{1,2} they have been utilized for various applications including traction motors of electric/hybrid vehicles.^{3,4} The coercivity of Nd-Fe-B magnets, however, has remained as small as about 1/3 of the anisotropy field.⁵ Solving this coercivity problem of Nd-Fe-B magnets is crucial for further progress in electric/hybrid vehicle applications. For this purpose, although a deeper understanding of the magnetization reversal process is imperative, it is very difficult because the magnetization reversal in Nd-Fe-B magnets takes place as multiple and simultaneous events of nucleation and domain wall depinning. Thus, we

believe that detecting these elemental magnetization reversal events is a direct way to understand the magnetization reversal process of Nd-Fe-B magnets.

The measurements of elemental magnetization reversal events in Nd-Fe-B magnets such as the Barkhausen effect have been attempted so far.^{6,7} This method, however, lacks quantitative accuracy. A direct method to detect the elemental magnetization reversal events in Nd-Fe-B magnets is to measure a micro-scale magnet sample with a very high-sensitivity magnetic measurement. As one of this approach, it was reported that a micro-patterned Nd-Fe-B magnet fabricated by a focused-ion beam (FIB) was measured by an X-ray magnetic circular dichroism (XMCD) technique.⁸ The FIB fabricated Nd-Fe-B

sample, however, regrettably lost its hard magnetic property due to the damage during the FIB process. In fact, it is well known that etching and/or polishing damages Nd-Fe-B sintered magnets significantly.^{9–11}

Contrary to the Nd-Fe-B sintered magnet, Nd-Fe-B hot-deformed (HD) magnets have high tolerance for process damages due to their very unique microstructure which consists of well aligned small platelet grains with several hundreds nm in diameter and several tens nm in thickness.^{12–18} The dominant magnetization reversal process in Nd-Fe-B HD magnets is considered to be the domain wall depinning through the studies of the detailed magneto-optical Kerr (MOKE) microscopy observation¹⁹ and the energy barrier analysis on coercivity.²⁰ Thus, when a Nd-Fe-B HD magnet is patterned into μm size range, it is highly expected to detect the elemental steps of domain wall depinning. Moreover, anomalous Hall effect (AHE) can be adopted for a sample of μm size range with sufficiently high sensitivity^{21–23} because AHE resistance R_{AHE} is inversely proportional to the sample thickness but is insensitive to the sample lateral size.

In this study, we have attempted to detect elemental steps of domain wall depinning in a micro-patterned Nd-Fe-B HD magnet using AHE detection technique. Firstly, MOKE microscopy observation was employed to recognize the magnetic domain structure of the Nd-Fe-B HD magnet, and the target size of the micro-patterning was discussed. Secondly, with carefully evaluating the process damage, the Nd-Fe-B HD magnet was thinned and micro-patterned by employing mechanical polishing and FIB processes. Consequently, the elemental steps of domain wall depinning were successfully detected.

II. EXPERIMENTAL

The sample used in this study is a standard Nd-Fe-B HD magnet with coercivity of 1.2 T. The magnetic domain structure of the sample was observed by using MOKE microscopy of Evico Magnetics¹⁹ for two samples having *ab* and *c* observing planes. The sample shapes are a rod of $1.8 \times 1.5 \times 2.5 \text{ mm}^3$ for *ab* observing plane and a plate of $1.7 \times 2.2 \times 0.6 \text{ mm}^3$ for *c* observing plane, respectively. The surfaces of these observing planes were prepared by the mirror polishing treatment.

The sample for the AHE measurements was fabricated as schematically shown in Fig. 1(a). The Nd-Fe-B HD magnet was cut out into a cube of 1 mm^3 with one plane parallel to *c*-plane. After polishing the plane parallel to the *c*-plane, the surface was covered with a Ta layer of 4 nm as an oxidation protection layer. Subsequently, the sample was flipped backside up and was fixed on a glass substrate, and it was thinned down to the thickness ranging from 100 to 5 μm by mechanical polishing. Then, a Ta layer of 4 nm again deposited on it. A Pt layer of 10 nm was deposited as an electrode on each of the four corners of the glass substrate, and the electrical contact between the sample and the Pt electrode was made using Ag paste. Finally, AHE cross-shaped micro-patterning was fabricated by FIB with the center width ranging from 140 to 13 μm . The FIB patterning was performed using the Ga ion beam of 30 kV and 45 nA with the diameter of 3 μm . The AHE measurement was performed with a current of 0.5 mA under the perpendicular field with respect to the sample plane using a superconducting magnet of 9 T at a maximum.

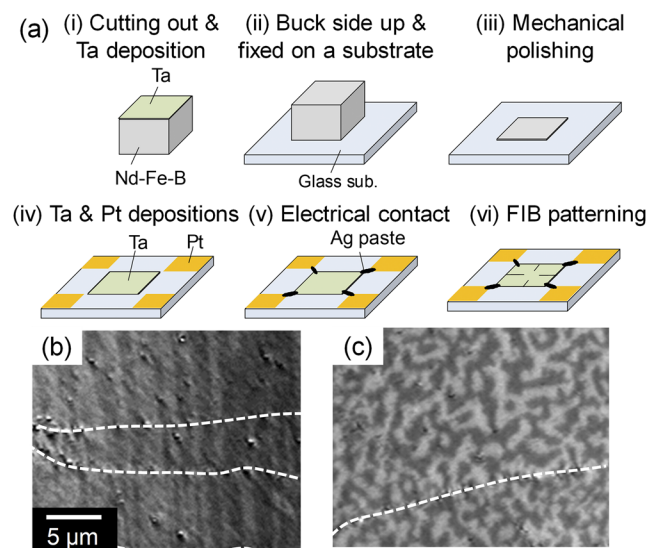


FIG. 1. (a) Schematic illustrations of the AHE cross micro-patterning procedure of the Nd-Fe-B HD magnet. MOKE images of thermally demagnetized (b) *ab*- and (c) *c*-planes, respectively.

III. RESULTS AND DISCUSSION

A. MOKE microscopy

Figures 1(b) and 1(c) show the MOKE images for the *ab*- and *c*-planes of the thermally demagnetized states. The magnetic domain is prolonged along the *c*-axis with the width of $1 \sim 2 \mu\text{m}$ and the length of about $30 \mu\text{m}$. The white broken lines in Figs. 1(b) and 1(c) represent the boundary of the original flake.²⁴ The flake thickness is about $10 \mu\text{m}$ perpendicular to the *c*-axis, thus, the magnetic domain runs through some of the flake boundaries along the *c*-axis. Since it has been reported that the $\text{Nd}_2\text{Fe}_{14}\text{B}$ grains near the flake boundary exhibit poor crystalline orientation,²⁵ our micro-patterning has to avoid the flake boundary. Therefore, the target thickness of the micro-patterning is determined to be less than $10 \mu\text{m}$. In the demagnetization process, a reversed domain nucleated at a certain field expands gradually as the demagnetizing field increases. From the careful MOKE observation of demagnetization process (not shown here), the sizes of the initial reversed domain and its expansion at each field are evaluated to be $(5 \mu\text{m})^2$ and $(1 \sim 2 \mu\text{m})^2$, respectively. These results indicate that only one reversed domain could exist in the detection area when the AHE cross is as small as $10 \mu\text{m}$. Thus, the lateral target size of the micro-patterning is determined to be $10 \mu\text{m}$.

B. AHE measurements

Figure 2(a) shows the AHE curves for the samples with various thickness before the FIB patterning. Note that R_{AHE} increases with decreasing the thickness, and very high sensitivity is confirmed even for the μm thickness range. The signal dispersion σ at the saturated region is evaluated as $0.006 \text{ m}\Omega$ for the $5 \mu\text{m}$ thick sample, indicating that the noise level of the AHE curve is $\sigma/R_{\text{AHE,sat}} = 0.0004$, where $R_{\text{AHE,sat}}$ is the saturation value of R_{AHE} . The inset of Fig. 2(a)

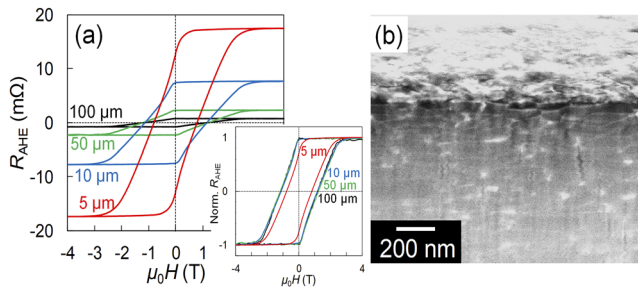


FIG. 2. (a) AHE curves of the samples of 100, 50, 10, 5 μm in thickness. Inset of (a) shows the normalized AHE curves with respect to the saturation. (b) Cross-sectional SEM image of the sample after mechanical polishing.

shows the normalized AHE curves. The AHE curve shape does not change in the range from 100 μm to 10 μm . This fact indicates that the effect of the surface damaged layer due to the mechanical polishing is negligible in this thickness range. On the other hand, the AHE curve for the thickness of 5 μm becomes narrower, and the coercivity decreases from 1.15 T to 0.8 T. This result suggests that the effect of the surface damaged layer becomes significant for the thickness of 5 μm . Figure 2(b) shows the cross-sectional SEM image of the surface region. Platelet grains with the size of ~ 300 nm in diameter and ~ 80 nm in thickness are confirmed whereas the crushed grain region is found at the surface. This surface damaged layer thickness is evaluated to be about 200 nm. Thus, the total thickness of the surface damaged layers for both the top and bottom sides is about 400 nm, indicating that about 10% of 5 μm thick sample loses the hard magnetic property. When the 10% topmost part of the AHE curve is removed, the coercivity recovers to 0.95 T. As this value of coercivity is slightly smaller than 1.15 T of much thicker samples, the soft magnetic property of the surface damaged layer affects to certain extent the magnetization reversal of the undamaged region of the 5 μm thick sample.

Figure 3(a) shows the optical microscopy image of the 5 μm thick sample with the FIB patterned AHE cross of 13 μm width. The AHE cross position denoted by the white broken line in Fig. 3(a) is selected to avoid the flake boundary as much as possible. Figure 3(b) shows the AHE curves of unpatterned, 140 μm , and 13 μm AHE cross width samples. Note that the AHE curve shapes are almost unchanged against the FIB patterning, indicating that the damage of FIB patterning is negligible. The coercivity for the sample with 13 μm AHE cross width increases slightly as compared with others. This may be attributed to the exclusion of the flake boundary inside the AHE cross. Moreover, the discrete steps are observed in the AHE curve of the sample with 13 μm AHE cross width as shown in Figs. 3(c) and 3(d). These are the enlarged AHE curve of the sample with 13 μm AHE cross width for the nucleation and the coercivity regions, respectively. In particular, the very large steps are observed for the nucleation region. As mentioned above, this region is the magnetization reversal of the surface damaged layer, indicating that the somewhat larger domains are formed in the surface damaged layer. On the other hand, many small steps are found near the coercivity region. The step height with respect to $R_{\text{AHE,sat}}$ near the coercivity region is about 0.002, which is still much larger

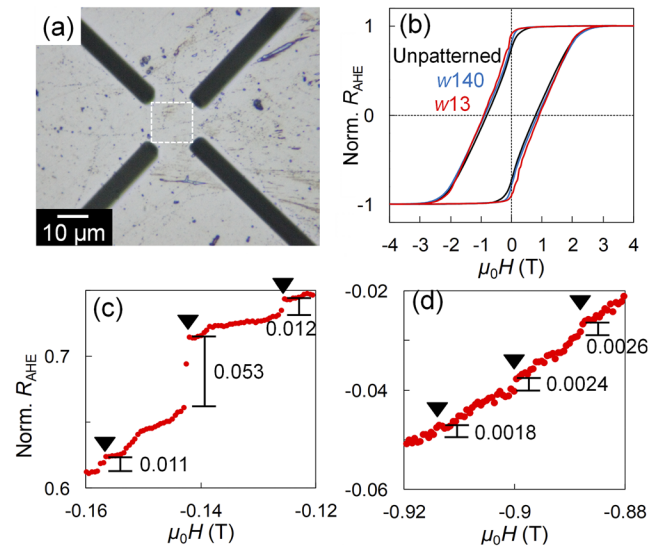


FIG. 3. (a) Optical microscopy image of the 5 μm thick sample with AHE cross width of 13 μm . (b) AHE curves of the unpatterned 5 μm thick sample and the FIB patterned one with AHE cross width of 140 μm and 13 μm . (c) and (d) are the enlarged AHE curves of the sample with AHE cross width of 13 μm for nucleation and coercivity regions, respectively. Triangle marks in (c) and (d) indicate the remarkable discrete steps.

than the noise level of $\sigma/R_{\text{AHE,sat}} = 0.0004$. Thus, it can be concluded that these steps correspond to the elemental steps of the domain wall depinning of the Nd-Fe-B HD magnet. If a vertically running domain wall as the MOKE microscopy images of Fig. 1(b) remains in the micro-patterned sample, the step heights with respect to $R_{\text{AHE,sat}}$ of 0.05, 0.01, and 0.002 observed the nucleation and coercivity regions correspond to the magnetization reversed area of $(2 \mu\text{m})^2$, $(0.9 \mu\text{m})^2$, and $(0.4 \mu\text{m})^2$, respectively. These values of the magnetization reversal areas are well consistent with those observed in the MOKE microscopy.

Finally, the removal of the surface damaged layer was tried. Ar-ion etching was employed to the 5 μm thick sample in which the coercivity reduction was significant. Figures 4(a) and 4(b) show the SEM images of the sample surface before and after etching. The etched thickness was about 300 nm. The sample surface before etching exhibits no clear contrast except for the scratching lines, whereas grain boundaries and voids are clearly observed after etching. Figure 4(c) shows the comparison of the AHE curves of the unetched 10 and 5 μm thick samples and the etched 5 μm thick sample. The reduction of the coercivity for the unetched 5 μm thick sample completely recovers by etching. Moreover, the nucleation field is slightly larger than that of the unetched 10 μm thick sample. This result clearly shows that the magnetic property and magnetization reversal process exhibit no degradation even in the thickness range of 5 μm when the surface damaged layer is removed. Thus, by combining the FIB patterning and Ar ion etching, the elemental magnetization events could be measured with keeping the magnetization reversal process of a bulk Nd-Fe-B HD magnet. By reducing the AHE cross area furthermore, the signal step height can be much larger, and the physical nature of the elemental magnetization reversal events

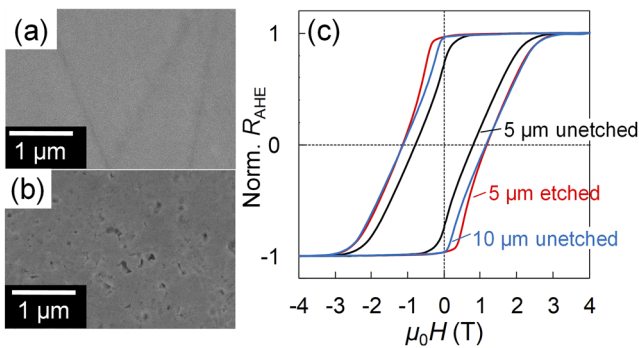


FIG. 4. (a) and (b) SEM images of the 5 μm thick sample surfaces before and after Ar ion etching. (c) AHE curves of unetched 10 μm thick, unetched 5 μm thick, and etched 5 μm thick samples.

will be unveiled by the stochastic analysis based on the Néel-Brown model.^{26–30}

IV. CONCLUSION

In this study, we have attempted to detect the elemental magnetization reversal events in a Nd-Fe-B hot-deformed magnet. For this purpose, the micro-patterned magnet sample was fabricated by means of the mechanical polishing and FIB patterning. The magnetization reversal of the sample was measured by AHE detection technique. Before the micro-patterning, the MOKE microscopy observation was performed for the c - and ab -planes, and the target size of the micro-patterning was determined to be 10 μm in both thickness and width. Subsequently, the sample was thinned down with carefully evaluating the effect of the surface damaged layer. Consequently, any deterioration of magnetic property was not found down to 10 μm thick while the coercivity decreased at 5 μm thick. This reduction of coercivity, however, was completely recovered by removing the surface damaged layer. The micro-patterned AHE cross sample was fabricated without showing any deterioration of magnetic property due to FIB damage. Discrete steps were observed on the AHE curve for the sample with 13 μm AHE cross width. Thus, we have successfully demonstrated to detect the elemental steps of magnetization reversal of the Nd-Fe-B hot-deformed magnet. Further reductions of sample thickness and AHE cross width will make the step signal much larger, and the physical nature of the magnetization reversal events will be analyzed in detail.

ACKNOWLEDGMENTS

FIB patterning was supported by Material Solution Center, Tohoku University. ESICMM (Grant Number 12016013) is funded by MEXT as a part of Element Strategy Initiative. This work was partially supported by Dynamic Alliance for Open Innovation Bridging Human, Environment and Materials from MEXT, the

Management Expenses Grants for National Universities Corporations from MEXT, JSPS KAKENHI Grant No. 17H03376, JST, Collaborative Research Based on Industrial Demand, and NIMS Joint Research Hub Program.

REFERENCES

- J. J. Croat, J. F. Herbst, R. W. Lee, and F. E. Pinkerton, *Appl. Phys. Lett.* **44**, 148 (1984).
- M. Sagawa, S. Fujimura, N. Togawa, H. Yamamoto, and Y. Matsuura, *J. Appl. Phys.* **55**, 2083 (1984).
- S. Sugimoto, *J. Phys. D: Appl. Phys.* **44**, 064001 (2011).
- Y. Matsuura, *J. Magn. Magn. Mater.* **303**, 344 (2006).
- M. Sagawa, S. Hirotsawa, H. Yamamoto, S. Fujimura, and Y. Matsuura, *Jpn. J. Appl. Phys.* **26**, 785 (1987).
- P. J. Thompson and R. Street, *J. Magn. Magn. Mater.* **171**, 153 (1997).
- M. LoBue, V. Basso, G. Beatrice, C. Bertotti, G. Durin, and C. P. Sasso, *J. Magn. Magn. Mater.* **290**, 1184 (2005).
- H. Yamamoto, I. Kitagawa, T. Kohashi, A. Sugawara, and T. Nishiuchi, *Hitachi-hyoron* **97**, 382 (2015) [in Japanese].
- D. Givord, P. Tenaud, and T. Viadieu, *J. Appl. Phys.* **60**, 3263 (1986).
- H. Nakamura, K. Hirota, M. Shimao, T. Minowa, and M. Honshima, *IEEE Trans. Magn.* **41**, 3844 (2005).
- D. Billington, K. Toyoki, H. Okazaki, Y. Kotani, T. Fukagawa, T. Nishiuchi, S. Hirotsawa, and T. Nakamura, *Phys. Rev. Mater.* **2**, 104413 (2018).
- J. J. Croat, J. F. Herbst, R. W. Lee, and F. E. Pinkerton, *J. Appl. Phys.* **55**, 2078 (1984).
- R. W. Lee, *Appl. Phys. Lett.* **46**, 790 (1985).
- R. K. Mishra, T. Y. Chu, and L. K. Rabenberg, *J. Magn. Magn. Mater.* **84**, 88 (1990).
- K. Hioki, A. Hattori, and T. Iriyama, *J. Magn. Soc. Jpn.* **38**, 79 (2013).
- J. Liu, H. Sepehri-Amin, T. Ohkubo, K. Hioki, A. Hattori, T. Schrefld, and K. Hono, *Acta Mater.* **61**, 5387 (2013).
- J. Liu, H. Sepehri-Amin, T. Ohkubo, K. Hioki, A. Hattori, T. Schrefld, and K. Hono, *Acta Mater.* **82**, 336 (2015).
- T. Yomogita, S. Okamoto, N. Kikuchi, O. Kitakami, H. Sepehri-Amin, T. Ohkubo, K. Hono, T. Akiya, K. Hioki, and A. Hattori, *J. Magn. Magn. Mater.* **447**, 110 (2018).
- M. Soderžnikz, J. Li, L. Liu, H. Sepehri-Amin, T. Ohkubo, N. Sakuma, T. Shoji, A. Kato, T. Schrefl, and K. Hono, *J. Alloys Compounds* **771**, 51 (2019).
- S. Okamoto, R. Goto, N. Kikuchi, O. Kitakami, T. Akiya, H. Sepehri-Amin, T. Ohkubo, K. Hono, K. Hioki, and A. Hattori, *J. Appl. Phys.* **118**, 223903 (2015).
- B. C. Webb and S. Schultz, *IEEE Trans. Magn.* **24**, 3006 (1988).
- S. Haan and J. C. Lodder, *J. Magn. Magn. Mater.* **168**, 321 (1997).
- N. Kikuchi, R. Murillo, and J. C. Lodder, *J. Magn. Magn. Mater.* **287**, 320 (2005).
- W. Grünberger, D. Hinz, A. Kirchner, K. H. Müller, and L. Schultz, *J. Alloys Compounds* **257**, 293 (1997).
- K. Hioki, T. Morita, A. Hattori, and T. Iriyama, *Denkiseiko* **86**, 83 (2016) [in Japanese].
- L. Néel, *Adv. Phys.* **4**, 191 (1955).
- W. F. Brown, *Phys. Rev.* **130**, 1677 (1963).
- W. Wernsdorfer, E. B. Orozco, K. Hasselbach, A. Benoit, N. Demoncey, A. Loiseau, H. Pascard, and D. Mailly, *Phys. Rev. Lett.* **78**, 1791 (1997).
- J. B. C. Engelen, M. Delalande, A. J. le Fèvre, T. Bolhuis, T. Shimatsu, N. Kikuchi, L. Abelmann, and J. C. Lodder, *Nanotechnology* **21**, 035703 (2010).
- S. Okamoto, T. Kato, N. Kikuchi, O. Kitakami, N. Tezuka, and S. Sugimoto, *J. Appl. Phys.* **103**, 07C501 (2008).